Title

55Mn-based fiducial markers for rapid and automated RF coil localization for hyperpolarized 13C MRI

Journal

Magnetic Resonance in Medicine, 85(1)

ISSN

0740-3194

Authors

Ohliger, Michael A

Gordon, Jeremy W

Carvajal, Lucas

et al.

Publication Date

2021

DOI

10.1002/mrm.28424

Peer reviewed

HHS Public Access

Author manuscript

Magn Reson Med. Author manuscript; available in PMC 2022 January 01.

Published in final edited form as:

Magn Reson Med. 2021 January ; 85(1): 518–530. doi:10.1002/mrm.28424.

^{55}Mn-based fiducial markers for rapid and automated RF coil localization for hyperpolarized ^{13}C MRI

Michael A. Ohliger[1], **Jeremy W. Gordon**[1], **Lucas Carvajal**[1], **Peder E. Z. Larson**[1], **Jao J. Ou**[2], **Shubhangi Agarwal**[1], **Zihan Zhu**[1], **Daniel B. Vigneron**[1], **Cornelius von Morze**[3]

[1]Department of Radiology and Biomedical Imaging, University of California San Francisco, San Francisco, California, USA

[2]Department of Radiology, Wake Forest School of Medicine, Winston Salem, North Carolina, USA

[3]Mallinckrodt Institute of Radiology, Washington University School of Medicine, St Louis, Missouri, USA

Abstract

Purpose: To use fiducial markers containing manganese 55 to rapidly localize carbon 13 (^{13}C) RF coils for correcting images for B_1 variation.

Methods: Hollow high-density polyethylene spheres were filled with 3M sodium permanganate and affixed to a rectangular ^{13}C-tuned RF coil. The relative positions of the markers and coil conductors were mapped using CT. Marker positions were measured by MRI using a series of 1D projections and automated peak detection. Once the coil location was determined, coil sensitivity was estimated using a quasistatic calculation. Simulations were performed to determine the minimum number of projections required for robust localization. Phantom experiments were used to confirm the accuracy of marker localization as well as the calculated coil sensitivity. Finally, in vivo validation was performed using hyperpolarized ^{13}C pyruvate in a rat model.

Results: In simulations, our algorithm was accurate in determining marker positions when at least 6 projections were used (RMSE 1.4 ± 0.9 mm). These estimates were verified in phantom experiments, where markers locations were determined with an RMS accuracy of 1.3 mm. A minimum SNR of 4 was required for automated detection to perform accurately. Computed coil sensitivity had a median error of 17% when taken over the entire measured area and 5.7% over a central region. In a rat, correction for nonuniform reception and flip angle was able to normalize the signals arising from asymmetrically positioned kidneys.

Conclusion: Manganese 55 fiducial markers are an inexpensive and reliable method for rapidly localizing ^{13}C RF coils and correcting ^{13}C images for B_1 variation without user intervention.

Keywords

coil sensitivity; fiducials; hyperpolarized carbon; manganese; RF coil

Correspondence: Michael A. Ohliger, Department of Radiology and Biomedical Imaging, University of California San Francisco, Box 0628, 1001 Potrero Ave, 1x55D, San Francisco, CA 94110, USA, Michael.ohliger@ucsf.edu, @michaelohliger.

1 | INTRODUCTION

RF surface coils are important for optimizing signal reception in emerging applications of hyperpolarized (HP) carbon 13 (^{13}C) MRI.[1–3] In HP ^{13}C MRI, dynamic nuclear polarization is used to increase the polarization of ^{13}C-labeled small molecules up to 100 thousand times more than is achievable by clinical MRI magnets.[4] Surface coil detection further improves the signals of ^{13}C probes. Moreover, arrays of surface coils can be used to provide greater coverage and be combined with parallel MRI to accelerate image acquisitions.

The principal drawback of using surface coils rather than volume coils is that their spatial reception patterns are nonuniform, impacting signal quantitation. Optimal image reconstruction with uniform spatial sensitivity requires knowledge of the coils' spatial sensitivity patterns.[5] Knowledge of coil sensitivities is also important for accelerated parallel imaging applications.[6–8]

Determining ^{13}C coil sensitivities is challenging. Direct measurement of the coil sensitivity patterns (a strategy often used in ^{1}H MRI) is precluded by the low endogenous ^{13}C signal in vivo. Enriched phantoms may be used for sensitivity measurement prior to the examination,[1] but this approach is not practical for arbitrary coil positioning as is typical for body imaging. "Self-calibrating" acquisitions have been proposed for integrating coil sensitivity measurement into the acquisition.[6] For accelerated acquisitions, these approaches decrease the achievable acceleration and are still not capable of determining the absolute coil sensitivities, which are required for accurately correcting metabolite signals as a function of distance from the coils.

One promising proposed approach for determining the sensitivities of ^{13}C coils has been direct electromagnetic field calculation.[9] The well-known principle of reciprocity in MRI states that the reception coil sensitivity of a RF coil can be calculated by considering the magnetic field, **B**, that would be generated by a unit current flowing through that coil.[10] The coil sensitivity, C(x), is related to this magnetic field, **B**(x), through the relation: $C(x) = B_x(x) - iB_y(x)$. Because ^{13}C has a relatively low frequency (32.1 MHz at 3 tesla [T]) and correspondingly long electromagnetic wavelength compared to the object being imaged, the magnetic field can be efficiently calculated using the quasi-static Biot-Savart approximation, which has an analytic solution for a finite conductor segment.

In order to effectively use this approach of direct calculation of coil sensitivities, it is necessary to accurately determine the locations of the conductor elements prior to acquisition. One proposed approach has been to use fiducial markers that can be imaged using proton MRI.[9] The disadvantage of proton-based fiducial markers is that they cannot be removed from the proton images, and localization of these markers either requires manually selecting the markers from a proton image or employing complicated image processing schemes. Fiducial markers based on resonant microcoils have been proposed[11]; however, these require specialized hardware.

We propose a method for automated localization of ^{13}C surface coils based on a novel system of manganese 55 (^{55}Mn)-based fiducial markers. ^{55}Mn is an NMR-active nucleus (spin-5/2) with resonant frequency very close to ^{13}C (offset by ~600 kHz at 3T), which can

be easily detected directly in its weakly paramagnetic +7 oxidation state.[12] This frequency is close enough to the ^{13}C resonant frequency to be excited using the same hardware as used to image ^{13}C but is outside the bandwidth of most ^{13}C imaging sequences. Therefore, these markers can be detected without any background signal and will not interfere with the HP ^{13}C acquisition.

In order to automate the localization process, we propose a system where 3 fiducial markers are placed on a RF coil with known coil geometry (measured using a CT scan). Localization of the markers is performed using a series of 1D projections, which lends itself to automation through peak detection. Once the coil location is determined, the coil sensitivity is computed using a Biot–Savart calculation. In this study, we describe the construction of this fiducial marker system as well as the algorithm used to locate the markers using a small number of projections. The robustness of this approach is demonstration using simulations with a large number of coil orientations. The calculated coil sensitivity determined by this approach is compared experimentally to that measured in a ^{13}C phantom. Finally, we demonstrate the feasibility of using this novel approach in vivo to obtain a uniform-sensitivity image reconstruction in an animal model during a HP ^{13}C acquisition.

2 | METHODS

2.1 | Overview

Coil localization using manganese markers is performed as follows (Figure 1): Three markers filled with ^{55}Mn are placed at various points along the conductor path of a ^{13}C-tuned RF coil. The exact positions of the markers are not important. However, it is ideal to avoid placing them in the configuration of an equilateral triangle (discussed below). A CT scan is then performed to determine the relative locations of the fiducial markers and the RF coil conductor elements. The endpoints of each conductor segment and fiducial are then used to generate a computational model of the RF coil (Figure 2). This step only needs to be performed once for each RF coil that is used.

At the time of the ^{55}Mn MR acquisition, the marker positions are measured by performing a series of 1D projections in which each marker represents a spectral peak. These projections are then mapped to determine the spatial locations of the markers within the MRI scanner. Knowing the locations of the markers and the calibration CT scan (described above), the location of the conductor path can be determined. Finally, a quasi-static computation of the magnetic field generated by each conductor element is used to determine the coil sensitivity.

In the sections below, we first describe the method of determining the marker locations from a series of projections, constrained by the known distance between markers. Next, we describe simulations used to determine the minimum number of projections required to localize 3 fiducial markers, followed by experimental evaluation of this technique, comparing the predicted RF coil sensitivity to a measured B_1 field map.

2.2 | Marker localization

Consider 3 fiducial markers that are located at positions r_1, r_2, and r_3. Next, consider n acquired projection direc-tions, denoted by the unit vectors s_1, s_2 … s_n. We construct 2 matrices, R and S, as:

$$R = \begin{bmatrix} | & | & | \\ r_1 & r_2 & r_3 \\ | & | & | \end{bmatrix} S = \begin{bmatrix} | & | & | & | \\ s_1 & s_2 & \cdots & s_n \\ | & | & | & | \end{bmatrix}. \quad (1)$$

The 1D expected projections along each direction are

$$P = S^{\dagger} R, \quad (2)$$

where † denotes the matrix transpose. The jth row of P, $p_j = \left[p_j^1, p_j^2, p_j^3\right]$, denotes the projection of the first, second, and third marker along the direction S_j. If we could measure P, then we could determine R using the pseudoinverse of $S^{\dagger}$.

Next, consider our measured peak locations along direction s_j, $\tilde{p}_j = \left\{\widetilde{p_j^1}, \widetilde{p_j^2}, \widetilde{p_j^3}\right\}$. Here, the braces {} denote a set of *unordered* elements. $\tilde{p}_j$ can have 1, 2, or 3 elements depending on whether the peaks from the 3 markers overlap. Note that we cannot directly determine p_j from the measured projections, $\tilde{p}_j$, because we do not know the order of the values that should make up p_j. In other words, although we know the projection locations, we do not know which measured projection was made from which marker. Therefore, determining the marker locations requires assigning each marker to the correct measured peak.

For a system of 3 fiducial markers, there are 6 possible ways to map the elements of each $\tilde{p}_j$ to p_j. This holds even if 2 of the markers overlap to form a single peak. Our proposed localization strategy amounts to considering all possible mappings and choosing the mapping that best fits 2 constraints: 1) known distances between fiducial markers, $r_m - r_n$, and 2) consistency with measured projections (Equation 2).

In order to map the marker projections to spatial locations, we first select a subset containing 3 of the acquired projections, $P^{\tilde{ref}} \equiv \left\{\tilde{p}_q, \tilde{p}_r, \tilde{p}_s\right\}$. These are considered "reference projections" and are the minimum number of projections to find an inverse to Equation (2). These projections correspond to a subset of the projection matrix $S^{ref} = \left\{s_q, s_r, s_s\right\}$. One simple way to choose the reference projections would be to use the projections along the x, y, and z axes. However, a more sophisticated method is proposed in Ref. 11. Reference projections are chosen by considering all possible sets of 3 projections, choosing the set of 3 that optimizes the following criteria: 1) determinant of S^{ref} is maximum; 2) number of overlapped peaks is minimized; and 3) distance between peaks is maximized.

Once the reference projections are chosen, we consider all possible ways of constructing $P^{\tilde{ref}}$ from the acquired projections. Because there are 6 possible peak assignments for each

projection and 3 reference projection directions, that gives a total of 6 × 6 × 6 = 216 possible assignments. Denote 1 of these 216 possible assignments as $P_{\alpha}^{\tilde{ref}}$. From this candidate assignment, we can determine a candidate configuration of markers

$$R_{\alpha} = inv\left(S^{ref-}\right)P_{\alpha}^{\tilde{ref}}, \tag{3}$$

where the columns of $R_{\alpha} = [r_1^{\alpha}, r_2^{\alpha}, r_3^{\alpha}]$ represent the candidate marker positions. We then compute the distance between markers in each candidate configuration, $d_{ij}^{\alpha} = r_i^{\alpha} - r_j^{\alpha}$, and compute the error function:

$$\Delta_{\alpha} = ij \neq \widetilde{\Sigma} d_{ij}^{\alpha} - d_{ij} + \sum_{i=1}^{n} \left(S^{\dagger} R_{\alpha}\right)_n - \tilde{p}_n . \tag{4}$$

The first term of the above equation computes the error in the inter-marker difference, and the second term computes the error in the measured projections. Because of the way R_{α} was constructed, the projection error will be 0 for the reference projections. However, the projection error will in general be non-zero for the nonreference projections. The marker configuration that minimizes Δ_{α} is selected as the best approximation of the true marker configuration.

To prevent spurious noise peaks from being incorporated into the reference projections, a further consideration is applied: if none of the candidate marker locations are able to match the distance constraint within 10 mm, a different projection is taken as the reference projection, P^{ref}.

2.3 | Simulations

We performed simulations to test the reconstruction algorithm and to determine the minimum number of projections required to accurately localize fiducial markers. A starting configuration of 3 fiducial markers, R^0, was chosen with similar dimensions to the RF coil we used in later experiments (see below). We then considered all possible orientations of the coil configuration by performing 3 successive rotations (Figure 3A):

$$R_i^0 = Rot_z(\phi) Rot_x(\theta) Rot_z(\alpha) R^0 . \tag{5}$$

In order to test all possible orientations, rotations were chosen randomly with a uniform distribution on a sphere by selecting 3 random variables, u_1, u_2, u_3, chosen from a uniform distribution 0 to 1, and defining the rotation angles as

$$\begin{aligned} \phi &= 2\pi u_1 \\ \theta &= \cos^{-1}(2u_2 - 1) . \\ \alpha &= 2\pi u_3 \end{aligned} \tag{6}$$

Given a proposed orientation, simulated projected marker locations were determined using Equation 2. In order to simulate the finite spatial resolution of our acquisition, peak locations were rounded to the nearest spectral position using the same parameters as our acquisition described below (313 points, 1.1 mm spatial resolution). A total of 10^6 different values for $[u_1, u_2, u_3]$ were considered.

We considered different numbers of projections, ranging from the 3 cardinal projections (x-, y-, z-axes), successively adding in 1 to 4 double oblique projections lying on the corners of a cube (Figure 3B). For each rotational state, we computed the RMSE between the predicted marker configuration based on our algorithm, R_i^{pred}, and the known starting configuration, R_i^0. We also computed the RMSE between the best possible marker configuration, R_i^{opt}, and the known starting configuration. Note that even in the best possible case the calculated marker configuration will not be exactly equal to the true maker configuration. This difference occurs because of the requirement that each of the projections is made into a discrete spectrum (e.g., spatial resolution is finite). We also determined how often the algorithm chose a configuration other than the "best" configuration and also how often the RMSE of the marker positions was greater than 3 mm.

2.4 | Fiducial markers

Fiducial markers were constructed using hollow spheres made from high-density polyethylene (Precision Plastic Ball Company, Franklin, IL). Importantly, high-density polyethylene material was selected based on its high resistance to oxidation by permanganate, which quickly oxidizes many organics. Spheres had external diameters of approximately 6.35 mm (0.25 inch) and inner diameters of approximately 4 mm. Spheres were filled with approximately 40 μL of 3M aqueous sodium permanganate ($NaMnO_4$) using a 27-gauge needle. Spheres were sealed using Teflon tape, which also resists oxidation (Figure 2A,B).

2.5 | RF coil

A rectangular RF coil consisting of solid tinned 16 AWG copper wire was constructed measuring 4.8 cm × 10 cm, tuned to the ^{13}C resonance frequency (32.1 MHz at 3T) and affixed to a plastic former. A passive ^1H RF block was constructed on the coil (on the opposite end of the ^{13}C active detuning circuit) to filter out signals at the ^1H frequency (128 MHz at 3T). Filled ^{55}Mn markers were placed along the conductor path at 3 different locations (Figure 2C).

2.6 | Conductor mapping

The locations of the coil conductor elements as well as the fiducial markers were measured by imaging the RF coil using a CT scanner (Lightspeed, GE Healthcare, Chicago, IL). The high-atomic number Mn solution could be clearly differentiated from the low-density high density polyethylene shell (Figure 2D). Images were exported into a DICOM viewer (Horos, The Horos Project). The endpoints of each conductor element were measured, as were the locations of each fiducial marker, and these were used to create a computational

model of the markers and conductor path (Figure 2E). Lumped elements such as inductors or capacitors were not included in the model.

2.7 | MRI acquisition

MR scanning was performed using a 3T clinical MR imager (Discovery 750, GE Healthcare), equipped with multi-nuclear capability. The RF coil was placed posterior to a head-shaped phantom that was filled with ethylene glycol (Figure 4A). An 8-channel RF coil array was used for ^{1}H MRI reception. In order to minimize any possible interactions, the ^{1}H coil array was removed from the scanner during ^{13}C acquisition. Note that in order to avoid disturbing the positioning of the ^{13}C coil, the ^{1}H RF coil was placed on the opposite (anterior) side of the phantom from the ^{13}C coil so it could be easily removed.

In order to measure the marker positions, a 1D projection acquisition was performed centered at the ^{55}Mn resonance frequency (31.7 MHz), with a 90° flip angle followed by a gradient-echo spatial encoding gradient. The direction of this spatial encoding gradient could be arbitrarily varied depending on the desired projection direction (actual directions used are described in the methods section below). Averaging was used where necessary. Acquisition parameters were as follows: readout bandwidth ±125 kHz; number of readout points = 313; readout gradient strength = 3.425 G/cm; TE = 5 ms; TR = 40 ms; spatial resolution = 1.1 mm/spectral point.

In order to obtain independent measurements of the fiducial marker positions, high-resolution T_2-weighted acquisitions were performed using a 3D fast spin echo acquisition (T_2 CUBE, matrix 384 × 384, echo train length 130, slice thickness 0.8 mm, slices 376, FOV 24 cm, voxel size 0.6 × 0.6 × 0.8 mm). T_2-weighted image were exported to a DICOM viewer for processing offline.

2.8 | Peak detection

Projection spectra were processed offline using MATLAB 2019a (MathWorks, Natick, MA). Peaks were detected automatically by finding all signals greater than 4 times the noise threshold. Subpixel localization was performed using Gaussian interpolation.[11] The spatial position was assigned by measuring the distance of each peak from the center of the spectrum and using a conversion factor of 1.1 mm/pixel.

2.9 | SNR dependence

A total of 7 projection directions were acquired: the 3 cardinal directions (*x*-, *y*-, and *z*-axes) as well as double-oblique projections corresponding to the corners of a cube. In order to determine the effects of SNR on spatial localization, data for each projection were obtained with either 128, 64, 32, 16, 8, or 4 signal averages. For each set of averages, the acquisition was repeated 8 times. For each projection, the SNR was measured by dividing the peak height by the SD of a signal-free region.

2.10 | B_1 field mapping

To characterize the surface coil and verify computed coil sensitivities, a B_1^+ map was acquired with the double angle method[13] using a head-shaped phantom containing natural

abundance ethylene glycol (Figure 4A). A single-band spectral-spatial RF pulse (130 Hz FWHM, 868 Hz stopband peak-to-peak) was used to excite the central resonance to avoid artifacts arising from chemical shift, and data were encoded using an echo planar sequence designed for ^{13}C imaging.[14] A single 20-mm thick slice was acquired with an in-plane voxel size of 5.0 mm × 5.0 mm (FOV = 80 mm × 80 mm, matrix 16 × 16), TR = 3s, TE = 24.6 ms, bandwidth = ±15.6 kHz, and echo spacing = 1.34 ms. The 2 nominal flip angles were $\alpha = 60°$ and $2\alpha = 120°$ (Figure 4B). To ensure sufficient SNR, 400 averages were acquired, yielding a total scan time of 40 minutes.

2.11 | Animal experiment

In order to validate our technique in vivo, a healthy Sprague–Dawley rat under isoflurane anesthesia was placed directly on the receiver coil in the lateral decubitus position such that 1 kidney was approximately 2 cm closer to the RF coil than the other. Animal studies were conducted according to approved protocol procedures of the University of California, San Francisco Institutional of Animal Care and Use Committee. Power was calibrated using an ethylene glycol phantom placed below the RF coil. [1-^{13}C]pyruvate was prepared, as previously described,[1] and polarized for approximately 120 minutes using a 5T SpinLab polarizer (GE Healthcare). After polarization, the sample was rapidly dissolved, and approximately 3 mL of the neutralized solution was injected into the rat tail vein. Metabolic ^{13}C images were then acquired dynamically using a spectrally selective echo planar imaging pulse sequence[14] with a fixed nominal flip angle on each metabolite (pyruvate 10 degree, lactate and alanine 30 degrees). Other scan parameters include: FOV = 12.8 cm, matrix 32 × 32, echo train length = 24 (75% partial-Fourier), TE = 21 ms, TR = 200 ms. Images were acquired every 3 s for a total time of 60 s. Fiducial marker locations were measured using 7 projections as described above.

After the data were reconstructed and the coil position determined, two corrections were applied. First, a $1/B_1$ correction was applied to account for the receive coil sensitivity. Second, a correction was performed to account for the nonuniform applied flip angle. In order to perform this correction, the flip angle was taken to be the nominal 10-degree flip angle (for pyruvate) when measured at a location, r_{ref}, which was the center of the phantom used for power calibration. The flip angle was calculated elsewhere according to the formula $\alpha(r) = \alpha(r_{ref})B_1(r)/B_1(r_{ref})$. Correction was then performed for the magnetization consumed during each RF excitation. That is, the *ith* time point was corrected by a factor $1/\left[\cos^{i-1}\alpha(r)\sin\alpha(r)\right]$.

3 | RESULTS

3.1 | Simulations

For 3 to 7 projections, the error of the best possible marker configuration ranged from 0.9 ± 0.15 mm (3 projections) to 0.97 ± 0.21 mm (4 projections) (Figure 5A). By contrast, the error in marker position determined from our algorithm ranged from 49.5 ± 8.5 mm (3 projections) to 1.4 ± 0.95 mm (6-7 projections). For 6 and 7 projection directions, therefore, the marker configuration chosen by our algorithm was close to optimal. In fact, for 6 and 7 projection directions, the optimal marker configuration was chosen by our algorithm 99%

of the time (Figure 5B), and the error in marker positioning was greater than 3 mm less than 0.001% of the time. Therefore, a minimum of 4 projections is necessary for accurate localization, with the most reliable results obtained when using 6 to 7 projections.

3.2 | Marker localization

All 3 markers were visible on the T_2-weighted FSE acquisitions (Figure 4C–E). Two of the markers (Figure 5C,D) showed much lower ^{1}H signal than the third (Figure 5A), suggesting less efficient filling with manganese. All 7 directions were acquired with adequate SNR for automatic peak detection (Figure 6A–G). Above each peak in Figure 6, the assignment of the 3 fiducial markers is shown, based on the algorithm described in the theory section. The predicted marker locations based on our algorithm differed from the measured locations based on T_2-weighed images by an RMS distance of 1.3 mm.

3.3 | SNR effects

In order to determine the effects of noise on marker location, we performed acquisitions with varying numbers of signal averages (4-128), each of which was repeated 8 times. The RMSE of the estimated marker position was relatively constant for 16 to 128 signal averages (Figure 7A). For 16 signal averages, there was slightly more variability, with the maximum RMS error reaching 3 mm. Using fewer than 16 averages, the accuracy of localization degraded dramatically. This threshold corresponds to a minimum SNR of the smallest peak of approximately 4 (Figure 7B) and occurs principally due to of false detection of peaks (noise is interpreted as a peak).

3.4 | Transient peak

When acquiring manganese spectra, we observed an intermittent transient peak occurring at approximately 2.4 kHz from ^{55}Mn (Figure 6G). The origin of this peak was uncertain, but it did not depend on the applied gradient and was not always suppressed through averaging. Because the peak location was independent of the applied gradients, we concluded it was unrelated to the sample. This peak most likely represented a local oscillator frequency within our scanner and, because it was always at the same frequency, was systematically ignored in our data processing.

3.5 | Computed and measured coil sensitivity

The computed coil sensitivity map, determined using the estimated conductor positions (Figure 8A,C), was qualitatively similar to the map measured using the double flip angle method (Figure 8B). Line profiles taken through the coil sensitivities also matched very closely (Figure 8D–F). The median error between the measured coil sensitivity and predicted coil sensitivity was 17% when taken over the entire measured area, and was 5.7% when considering a 2 × 2.5 cm central region corresponding to the most sensitive volume of the coil (yellow rectangle in Figure 8C).

3.6 | Animal experiment

The proposed technique was tested in vivo by placing a healthy rat on its side and comparing the signals detected in the 2 kidneys (Figure 9). Without any B_1 correction (Figure 9D,G),

the average signal in the kidney closer to the coil (“down” kidney) was 23.9 ± 20, whereas the average signal in the kidney further from the coil (“up” kidney) was 8.23 ± 5.10. The distance between the kidneys was approximately 2 cm. Using the computed coil sensitivity to correct only the receive profile (Figure 9E,H), there was less difference between the 2 kidneys (down: 24.3 ± 19, up: 17.8 ± 11.0). Finally, when the computed coil sensitivity was used to correct both the receive profile as well as the flip angle (Figure 9F,I), the difference in total pyruvate was only 14% (down: 13.1 ± 10, up: 15.0 ± 10).

4 | DISCUSSION

We have developed a method of rapid and automated localization of ^{13}C RF surface coils using a system of ^{55}Mn fiducial markers, followed by Bj correction. Localization is based on a series of 1D projections, which are combined with known measurements of the intermarker distances made by a separate CT scan of the RF coil. The CT scan is also used to map the positions of the coil conductors relative to the fiducial markers. For a rigid RF coil, this relationship is fixed; therefore, the calibration CT scan needs to be performed only once. The coil sensitivity is determined using a quasi-static calculation based on the Biot-Savart law, which can be solved in closed form and rapidly computed for individual conductor elements. The estimated coil sensitivity using our approach closely matches a direct measurement of the B_1 field of our RF coil obtained using the double flip angle technique.

We have also demonstrated the effectiveness of this technique in vivo by correcting both the receive coil sensitivity profile and the applied flip angle in order to restore symmetry in the HP ^{13}C pyruvate signals derived from rat kidneys. Because dynamic HP ^{13}C experiments consume polarization during every excitation, having a correct estimation of the flip angle is crucial for accurate signal quantification. This effect is expected to be most pronounced when the same surface coil is used for transmission and reception.

Fiducial marker systems have previously been proposed for locating ^{13}C RF coils and performing sensitivity corrections.[9] This approach was able to successfully correct for coil sensitivity variations. However, because ^{1}H fiducial markers were used, manual identification of marker locations was required. Because our approach is based on 1D projections without any background signal, it is easily automated using peak detection.

A similar approach to coil localization based on projections was describe in Ref.11 In that work, specially tuned RF microcoils were used to obtain the projections. Although the use of microcoils offers flexibility and high SNR, it requires specialized hardware for detection. By contrast, ^{55}Mn-based markers are inexpensive (approximately $5 USD each) and can be detected using existing ^{13}C hardware. The use of fiducial markers with a distinct chemical shift (induced by ethanol and acetone solvents) in phosphorus spectroscopy has also been previously described.[15]

Through simulations, we determined that at least 4 projection directions were sufficient for accurate localization. It is interesting to note that using only 3 projections lead to large errors. This is expected because when the coil lies in the same plane as the projection axes

(the *x*–*y* plane in this case), there are orientations where the "correct" orientation has the same projections as its mirror image. Using at least 4 projections breaks this symmetry.

The minimal number of required projections that we determined are lower than the minimal number of projections found in Ref. 11. However, Ref. 11 determined peak locations only from the individual projections. We were able to obtain accurate results with fewer directions by additionally considering the known intermarker distances. In the future, the number of required projections could potentially be further reduced by making the markers more distinguishable, for example, by filling each marker with different amounts of ^{55}Mn.

We noted an artifactual peak due a "transient" signal that appeared in our spectra at a fixed spectral position. The origin of this peak was uncertain but was likely related to a poorly isolated signal within the MRI system electronics. In our implementation, because the peak was always at a fixed frequency and had a narrow band, this could easily be removed from our spectra prior to processing. However, this approach could potentially present problems if the signal overlapped a "true" peak. One possible solution would be to avoid placing coils such that the marker is at this "magic" position (in our case close to isocenter). A more general solution would be to acquire spectra in an alternating fashion with the readout gradient reversed. "True" peaks will reflected around the 0 position, whereas the transient peak stays in the same place.

The accuracy of marker localization depends on the SNR of the acquired projections. Because the marker position is measured using the location of each projection peak and not the height, we require only that the SNR of each peak is sufficient to be detected above the noise floor. For our system, at least 16 signal averages were required for each projection, corresponding to a minimal SNR of 4 for the smallest peak. With a TR of 40 ms, this would lead to an acquisition time of 640 ms × 7 projections = 4.5 s for accurate localization. Note also that 2 of our 3 markers were only partially filled with manganese (Figure 2), leading to a smaller peak. We anticipate that with an improved filling technique, we could increase the SNR of acquired peaks, further decreasing the time required to obtain a full set of projections.

For this initial work, we considered a system of only 3 fiducial markers placed at fixed locations around an RF coil. Three markers were chosen because this is the minimum number of points necessary to establish the location and orientation of a planar radiofrequency coil. The distribution of markers was chosen to maximize the separation of markers while keeping them close enough to the coil to provide adequate signal. We have not systematically investigated the placement of the markers. However, it is important that the sides of the triangle formed by the 3 markers should be different lengths. If 2 sides are of equal length and the triangle has an axis of symmetry, then a given configuration of markers cannot be distinguished from its reflection. Therefore, an RF coil placed "upside down" (with conductors on the opposite side of the image plane) will have the same projections as a coil placed in the correct orientation.

In addition to RF coil localization, this approach is potentially valuable for monitoring *subject* motion during an acquisition. There is increasing interest in using optical markers

to track the motion of subjects during an MRI scan in order to perform perspective motion correction.[16,17] Manganese markers could facilitate rapid motion tracking without the external hardware required for optical approaches.

Although being able to correct the sensitivity of a single RF coil is useful, it would be advantageous to extend this approach to RF coil arrays in order to take advantage of accelerated parallel imaging techniques. This extension to coil arrays is relatively straightforward; however, several challenges are anticipated: First, because the number of markers is increased, the localization algorithm becomes more complex. Additionally, inductive coupling of ^{55}Mn signals between coil elements will need to be considered. Finally, our approach assumes linear gradients, and because many coil arrays are used at the edges of the MR scanner volume, nonlinearities in gradients will need to be accounted for. Finally, our analysis does not spatially assess the phase of the computed coil sensitivity. Accuracy of the individual coil phase shifts, including the effects of electronics and cable lengths, can be important to achieve optimal combinations of coil array data, especially with computed coil sensitivities.[15]

5 | CONCLUSION

A rapid, automated method for localization of ^{13}C RF coils has been developed based on ^{55}Mn fiducial markers. This will permit correction for coil sensitivity variations in HP ^{13}C acquisitions, allowing for more accurate metabolic imaging using surface coils.

ACKNOWLEDGMENT

This work was supported by the National Institutes of Health (NIDDK 5R01115987 and NIBIB P41EB013598).

Funding information

This work was supported by the National Institutes of Health (NIH)/National Institute of Diabetes and Digestive and Kidney Diseases (NIDDK) grants 5R01115987 and NIBIB P41EB013598

REFERENCES

1. Park I, Larson PEZ, Gordon JW, et al.Development of methods and feasibility of using hyperpolarized carbon-13 imaging data for evaluating brain metabolism in patient studies. Magn Reson Med. 2018;80:864–873. [PubMed: 29322616]
2. Nelson SJ, Kurhanewicz J, Vigneron DB, et al.Metabolic imaging of patients with prostate cancer using hyperpolarized [1-13C]pyruvate. Sci Transl Med. 2013;5:198ra108.
3. Cunningham CH, Lau JY, Chen AP, et al.Hyperpolarized 13C metabolic MRI of the human heart: Initial experience. Circ Res. 2016;119:1177–1182. [PubMed: 27635086]
4. Ardenkjaer-Larsen JH, Ardenkjaer-Larsen JH, Fridlund B, et al.Increase in signal-to-noise ratio of >10,000 times in liquid-state NMR. Proc Natl Acad Sci USA. 2011;100:10158–10163.
5. Roemer PB, Edelstein WA, Hayes CE, Souza SP, Mueller OM. The NMR phased array. Magn Reson Med. 1990;16:192–225. [PubMed: 2266841]
6. Ohliger MA, Larson PEZ, Bok RA, et al.Combined parallel and partial fourier MR reconstruction for accelerated 8-channel hyperpolarized carbon-13 in vivo magnetic resonance Spectroscopic imaging (MRSI). J Magn Reson Imaging. 2013;38:701–713. [PubMed: 23293097]
7. Tropp J, Lupo JM, Chen A, et al.Multi-channel metabolic imaging, with SENSE reconstruction, of hyperpolarized [1-13C] pyruvate in a live rat at 3.0 Tesla on a clinical MR scanner. J Magn Reson. 2011;208:171–177. [PubMed: 21130012]

8. Arunachalam A, Whitt D, Fish K, et al.Accelerated spectroscopic imaging of hyperpolarized C-13 pyruvate using SENSE parallel imaging. NMR Biomed. 2009;22:867–873. [PubMed: 19489035]
9. Dominguez-Viqueira W, Geraghty BJ, Lau JYC, Robb FJ, Chen AP, Cunningham CH. Intensity correction for multichannel hyperpolarized 13C imaging of the heart. Magn Reson Med. 2015;75:859–865. [PubMed: 26619820]
10. Insko EK, Elliott MA, Schotland JC, Leigh JS. Generalized reciprocity. J Magn Reson. 1998;131:111–117. [PubMed: 9533912]
11. von Morze C, Carvajal L, Reed GD, Swisher CL, Tropp J, Vigneron DB. Magnetic resonance imaging. Magn Reson Imaging. 2014;32:1165–1170. [PubMed: 25179135]
12. Galassi F, Brujic D, Rea M, Lambert N, Desouza N, Ristic M. Fast and accurate localization of multiple RF markers for tracking in MRI-guided interventions. Magn Reson Mater Phy. 2014;28:33–48.
13. Stollberger R, Wach P. Imaging of the active B1 field in vivo. Magn Reson Med. 1996;35:246–251. [PubMed: 8622590]
14. Gordon JW, Vigneron DB, Larson PEZ. Development of a symmetric echo planar imaging framework for clinical translation of rapid dynamic hyperpolarized (13) C imaging. Magn Reson Med. 2017;77:826–832. [PubMed: 26898849]
15. Rodgers CT, Robson MD. Coil combination for receive array spectroscopy: Are data-driven methods superior to methods using computed field maps?Magn Reson Med. 2015;75:473–487. [PubMed: 25820303]
16. Zahneisen B, Keating B, Ernst T. Propagation of calibration errors in prospective motion correction using external tracking. Magn Reson Med. 2013;72:381–388. [PubMed: 24123287]
17. Singh A, Zahneisen B, Keating B, et al.Optical tracking with two markers for robust prospective motion correction for brain imaging. Magn Reson Mater Phy. 2015;28:523–534.

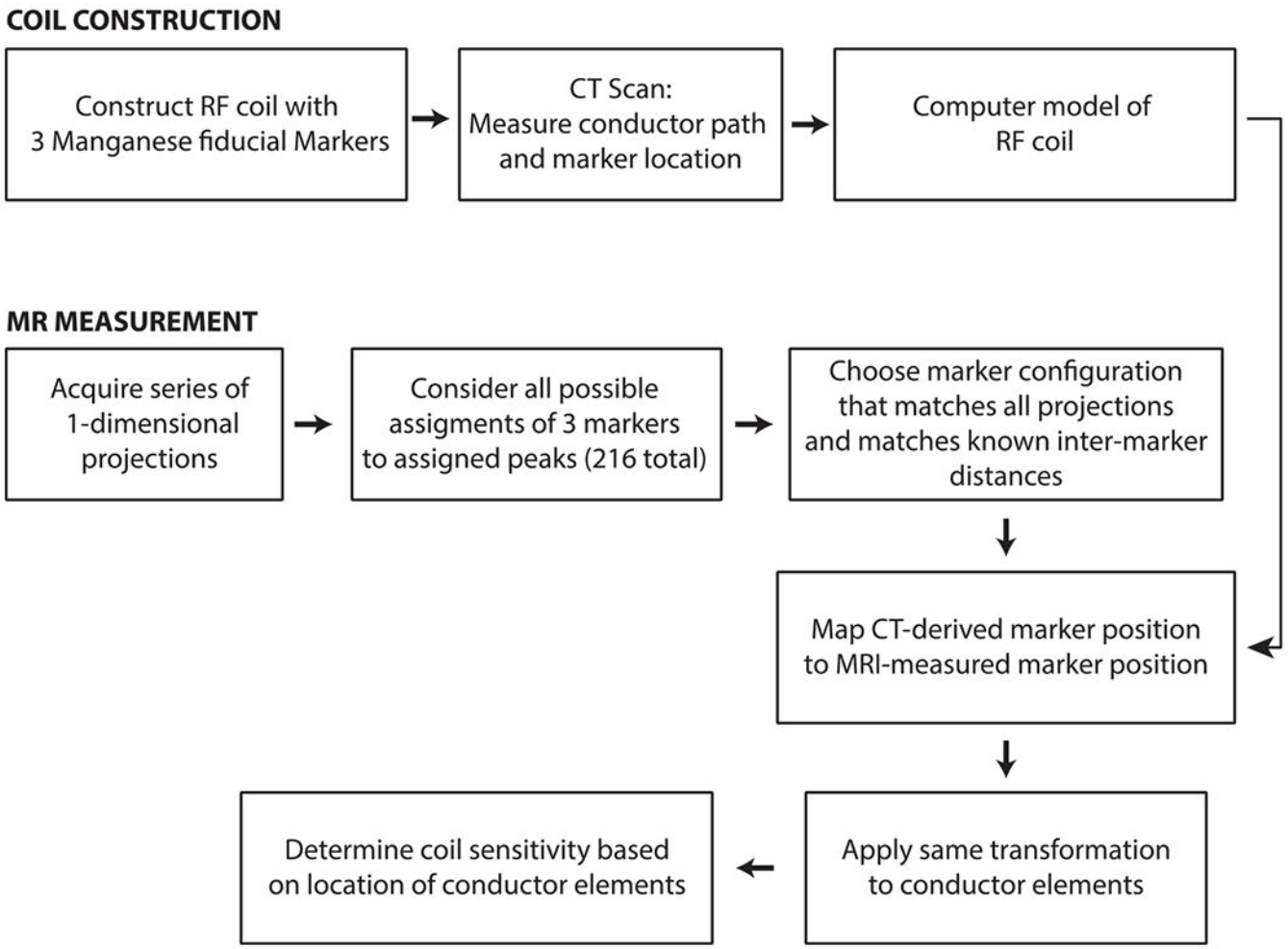

FIGURE 1.
Schematic approach for determining the location of RF coil and coil sensitivity using ^{55}Mn fiducial markers and 1D projections. ^{55}Mn, manganese 55

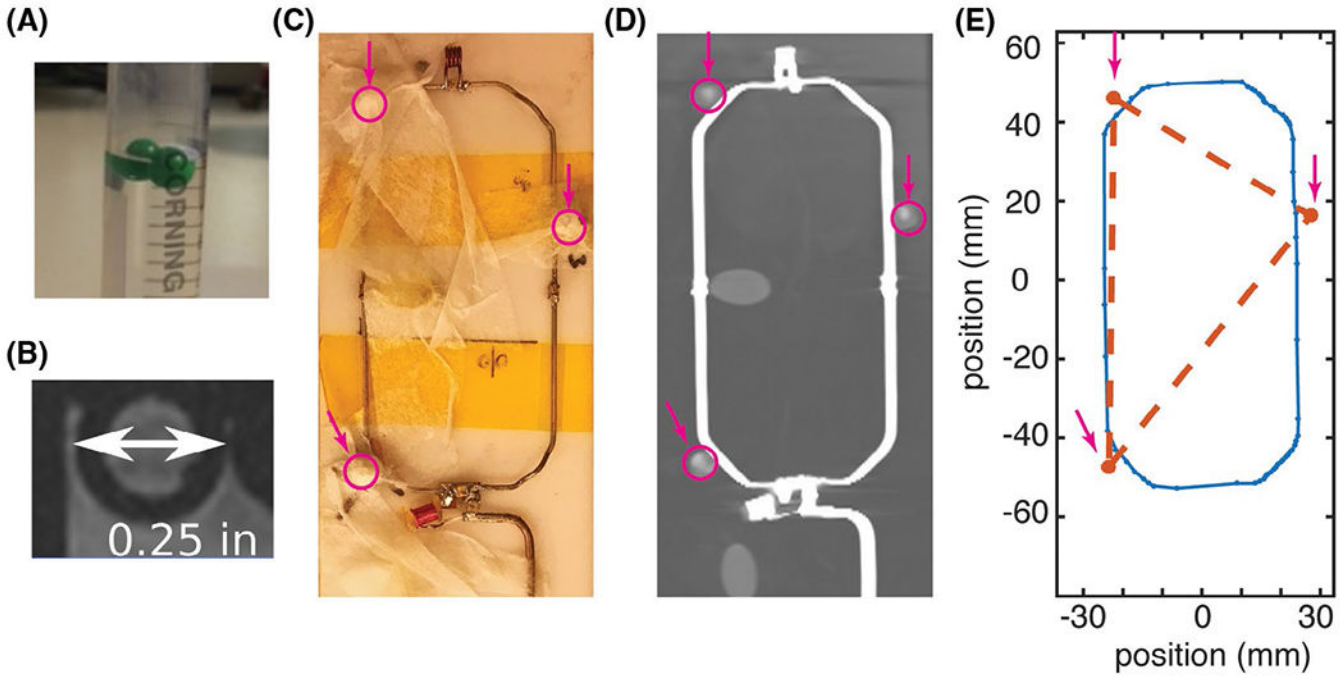

FIGURE 2.

(A) High-density polyethylene spheres used as markers. (B) Spoiled gradient-echo MR image of a single hollow marker filled with saline and placed in a saline bath for illustration purposes. The signal void represents the thickness of plastic used in the markers. (C) RF coil used for phantom studies, with pink circles and arrows illustrating the location of fiducial markers (markers appear white because they are wrapped in Teflon tape). (D) Single coronal slice from a CT scan used to measure marker positions and coil conductor locations. Pink arrows and circles again show the marker locations. (E) Computational model of the coil conductor path as well as the relative locations of fiducial markers, as extracted from the CT scan

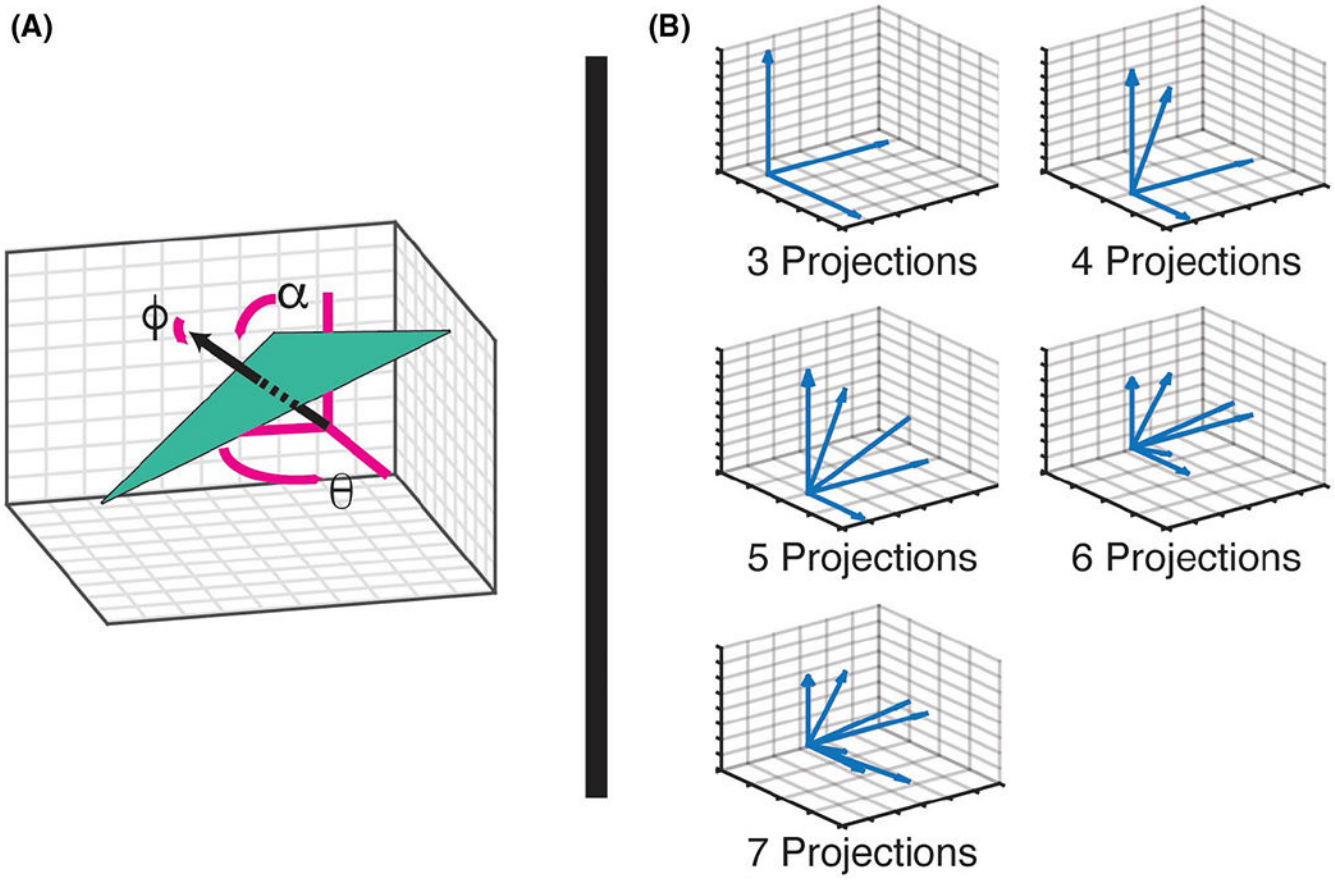

FIGURE 3.

(A) Three axes of rotation used to test different orientations of the RF coil and fiducial markers in simulations. (B) Projection directions tested as part of simulations. Three cardinal axes were used (*x*-, *y*-, *z*-), with successive addition of the corners of a cube

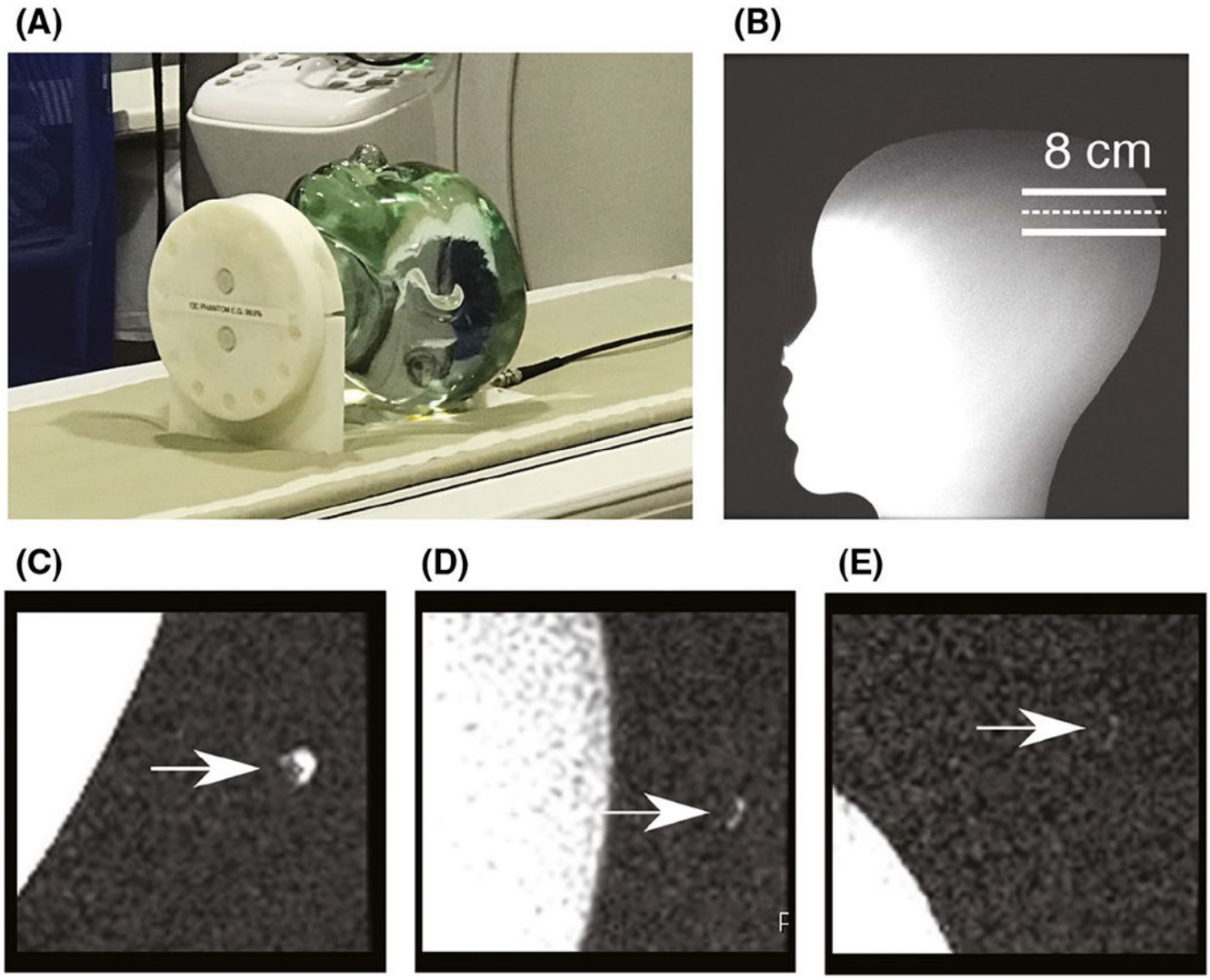

FIGURE 4.

(A) Experimental setup with ethylene glycol phantom placed on top of RF coil. (B) T_2-weighted fast spin echo image of the ethylene glycol phantom illustrating the imaging plane used for coil sensitivity determination. The signal variation within the phantom is caused by the placement of the proton RF coil on the anterior aspect of the phantom. (C-E) T_2-weighted images of the fiducial markers used to confirm the accuracy of ^{55}Mn-based measurements. Arrows point to the markers. Varying signals obtained from each marker reflects varying efficiency of marker filling

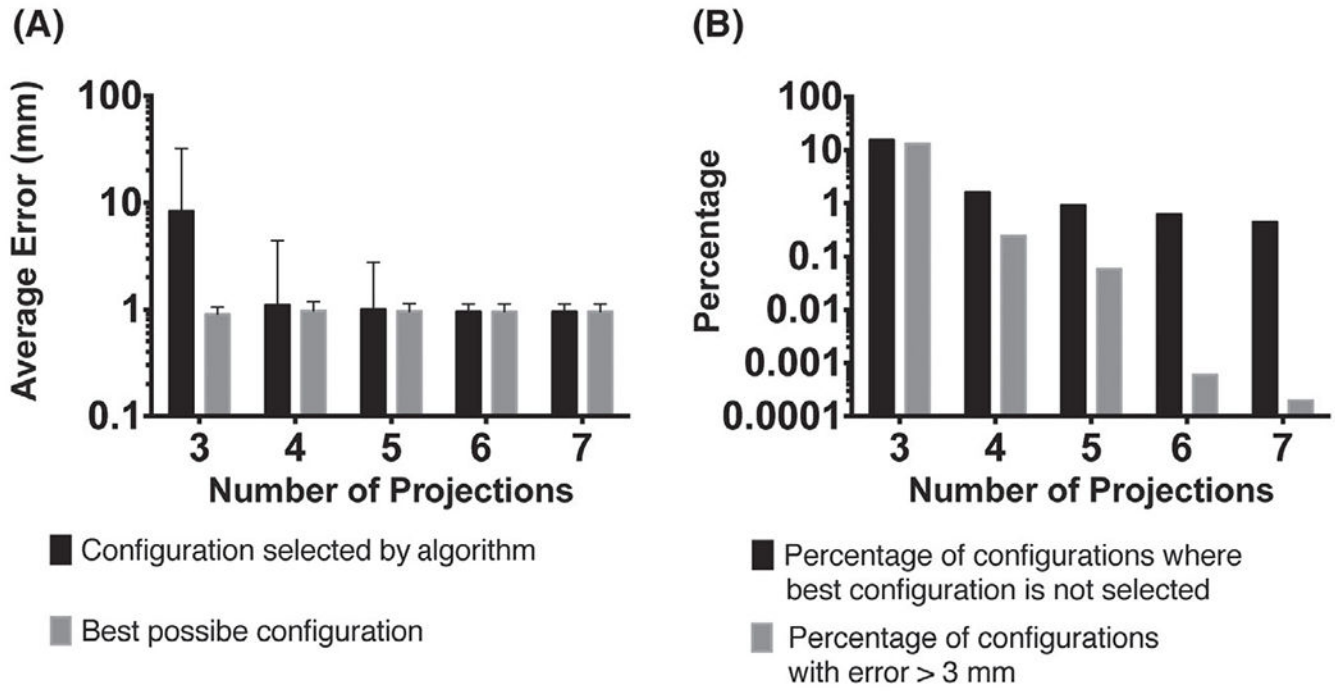

FIGURE 5.

(A) RMS error in marker locations determined by simulations over 10^6 randomly determined coil orientations using varying numbers of 1D projections (see Figure 3). Black bars = RMS error of marker configuration selected by the proposed algorithm. Gray bars = RMS error of best possible marker configuration. Error bars are SD taken over all coil rotations considered. (B) Black bars = percentage of simulated coil orientations where the proposed algorithm failed to select the best possible marker configuration. Gray bars = percentage of simulated coil orientations where the RMS error in marker positions determined by the proposed algorithm was greater than 3 mm

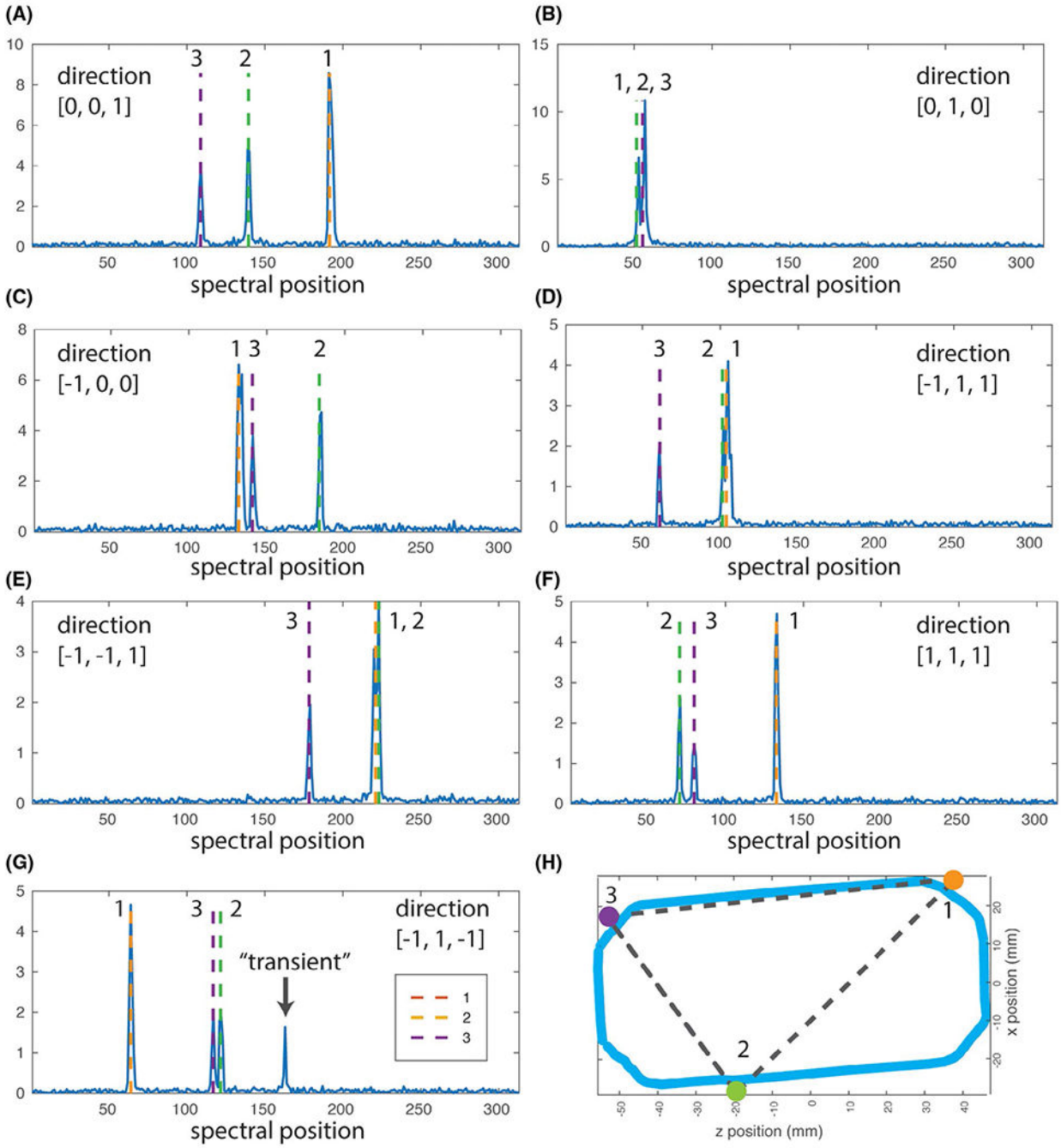

FIGURE 6.

(A-G) 1D projections of fiducial markers using the coil setup shown in Figure 4A. Peaks are identified from our algorithm as coming from 1 of 3 fiducial markers (shown in H). (G) Location of a spurious peak that occurred in sporadically in select experiments, likely contamination from MR scanner hardware (see Section 3.4)

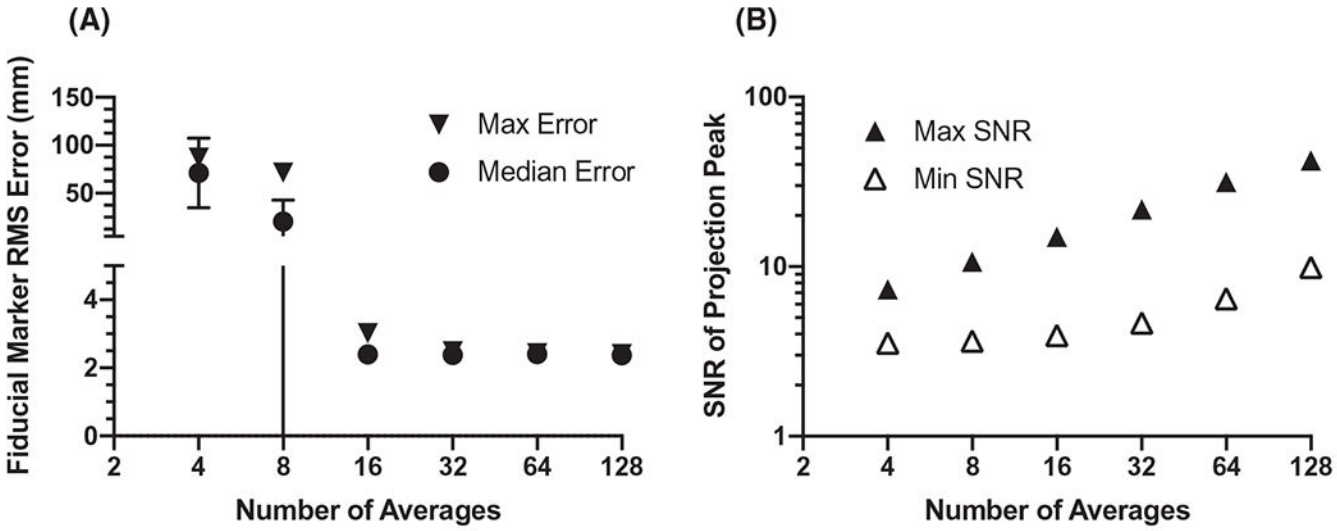

FIGURE 7.

(A) RMS error in fiducial marker location as a function of the number of averages taken for 1D projections (B) Minimum (triangle) and maximum (square) SNR of all measured peaks as a function of number of averages used to create 1D projections. Error bars are the SD taken over 8 repetitions. Where error bars are not shown, the SD is smaller than the marker size

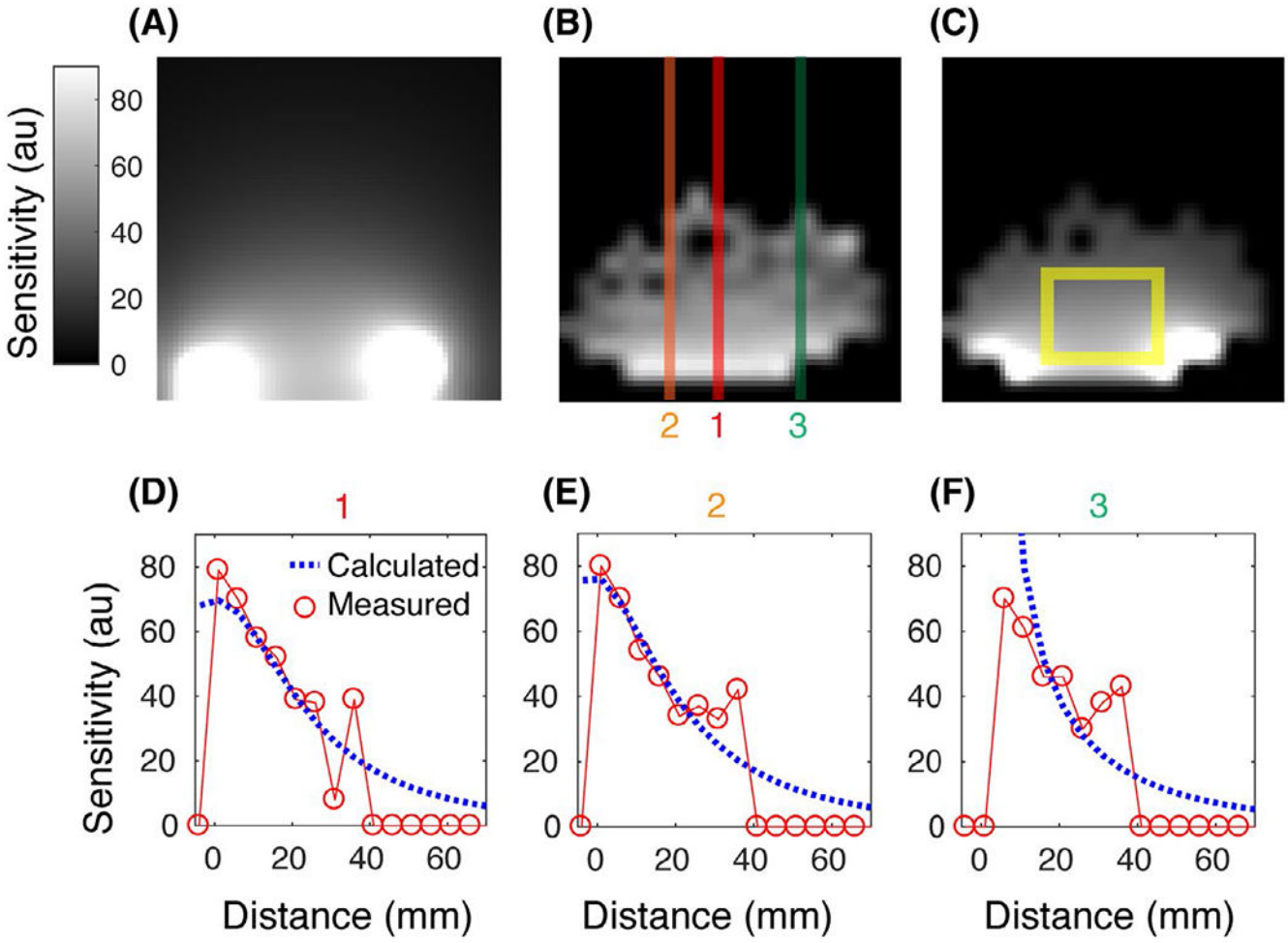

FIGURE 8.

(A) Coil sensitivity calculated for the RF coil tested along the image plane shown in Figure 4B. (B) Coil sensitivity measured using double flip angle method, masked where there is minimal acquired signal. Note the round shape of the phantom that is visible. Red lines show the line profiles used to generate the plots in D-F. (C) Calculated coil sensitivity with the same masking as show in B. Yellow rectangle illustrates the central region used to compare sensitivity values (see Section 3.5). (D-F) Line profiles comparing the calculated (blue dashes) and measured (red circles) coil sensitivities. Locations of line profiles are shown in B

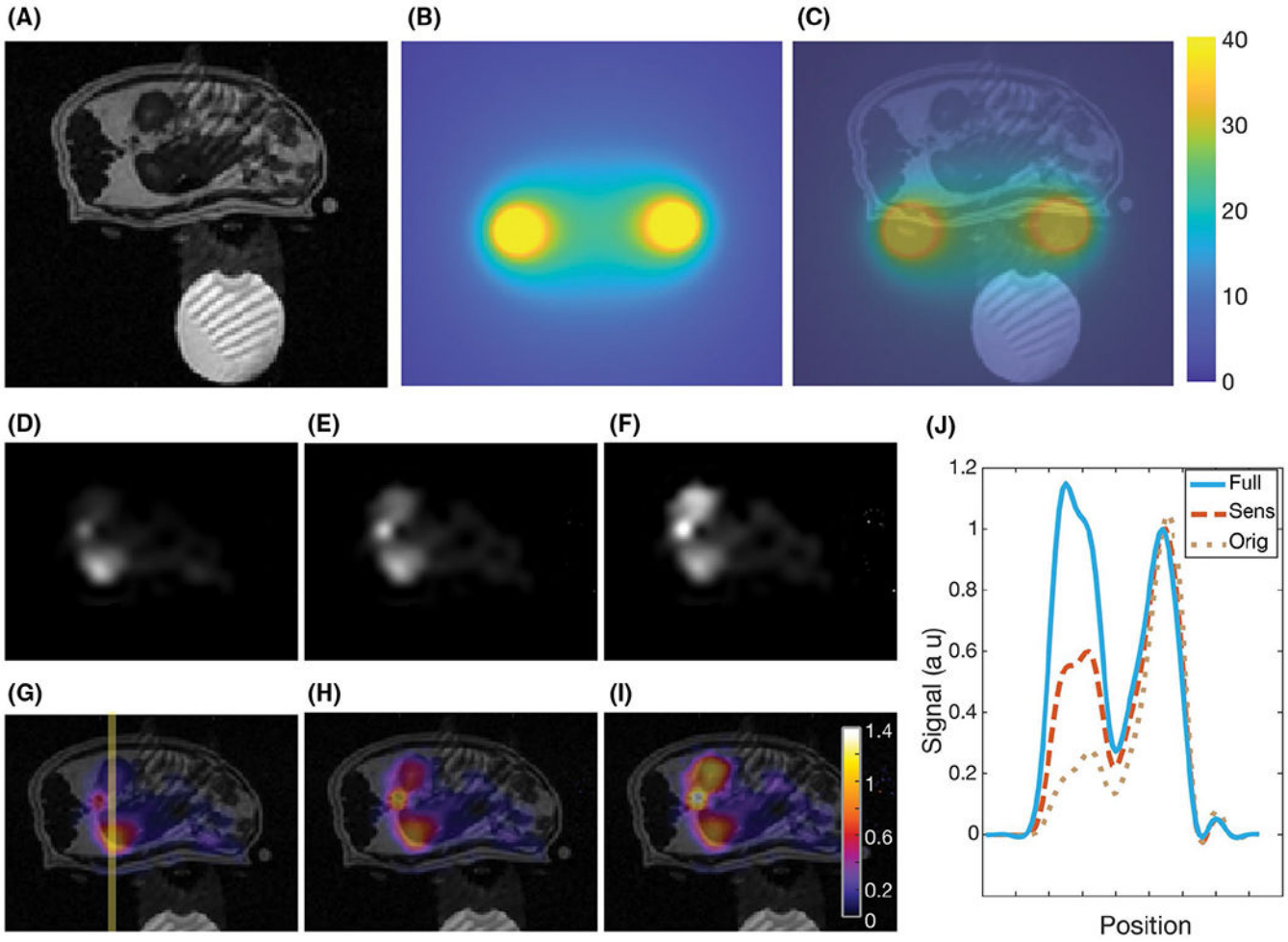

FIGURE 9.

(A) In vivo rat experiment setup. Rat was placed on its side, with RF coil immediately below the rat. Phantom used for calibration is located on the opposite side of the RF coil. (B) Flip angle map (degrees) calculated based of fiducial marker localization. (C) Flip angle map overlayed on the anatomic image. (D,G) Total pyruvate signal displayed without any coil correction. (E,H) Total 13C pyruvate signal after correcting only for the RF coil's reception coil profile. (F,I) Total 13C pyruvate signal after correcting for both the reception profile and nonuniform flip angle. (J) Line profile taken through the kidney (shown as yellow line in G) comparing the uncorrected and corrected ^{13}C pyruvate signal